

Object selectivity of local field potentials and spikes in the macaque inferior temporal cortex

Gabriel Kreiman^{1,2,3,4*#}, Chou P. Hung^{1,2,4*}, Alexander Kraskov⁵, Rodrigo Quijan Quiroga⁶, Tomaso Poggio^{1,2,3,4}, James J. DiCarlo^{1,2,4}

¹ McGovern Institute for Brain Research,

² Center for Biological and Computational Learning,

³ Computation and Systems Biology Initiative,

⁴ Department of Brain and Cognitive Sciences, Massachusetts Institute of Technology

⁵ Division of Biology, California Institute of Technology

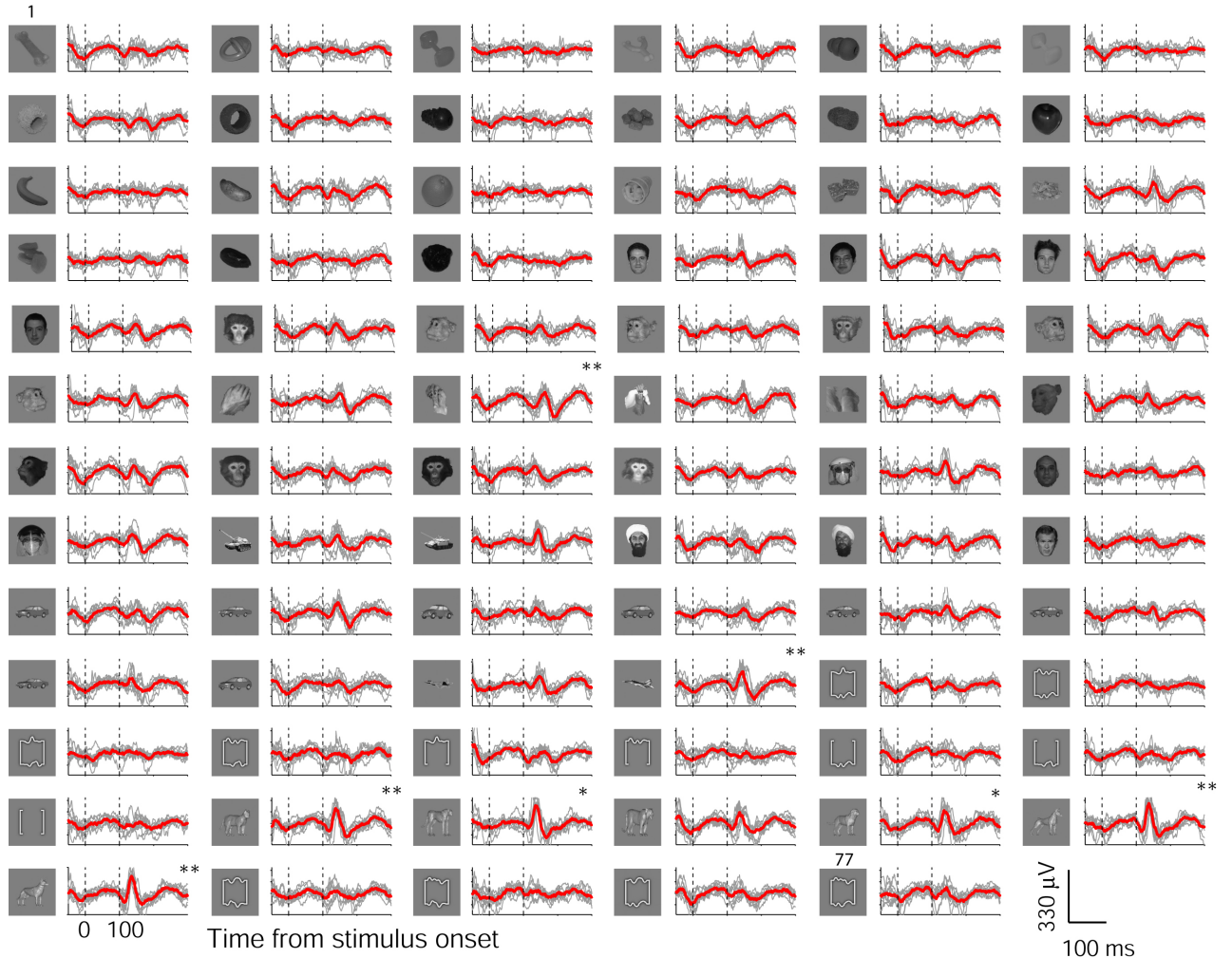
⁶ Dept. of Engineering, University of Leicester, UK

* These authors contributed equally to this work

To whom correspondence should be addressed at kreiman@mit.edu

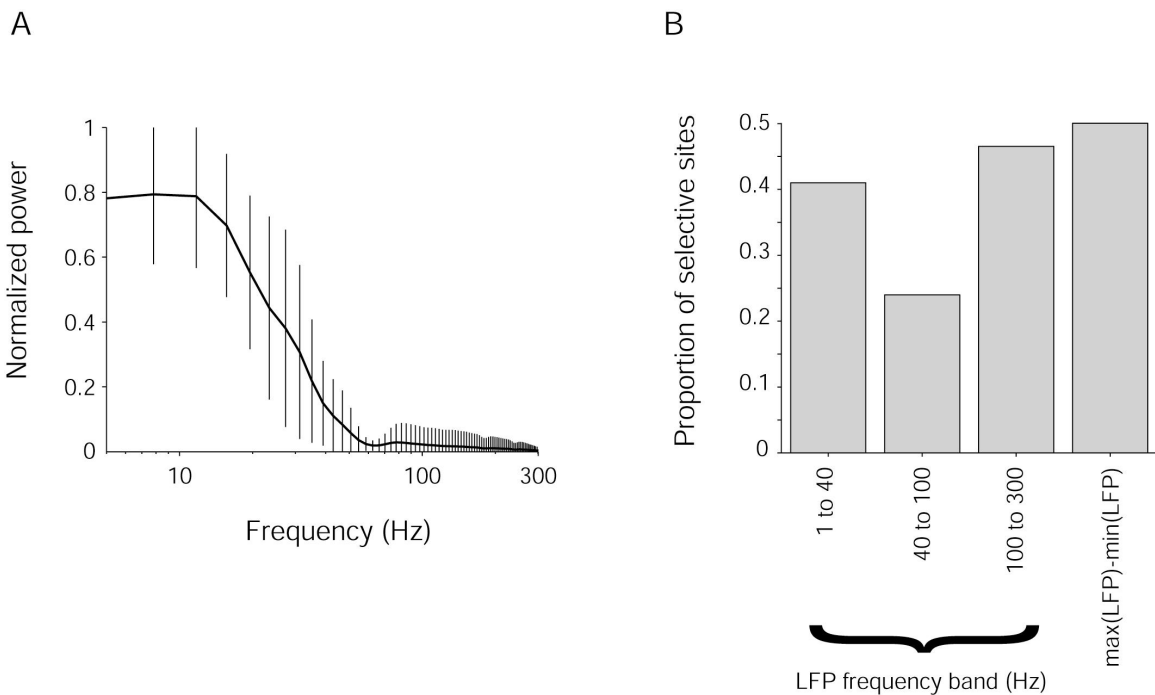
Additional Supplementary Material is available at

<http://ramonycajal.mit.edu/kreiman/resources/lfps/>



Supplementary Figure 1: Example of selectivity in LFPs

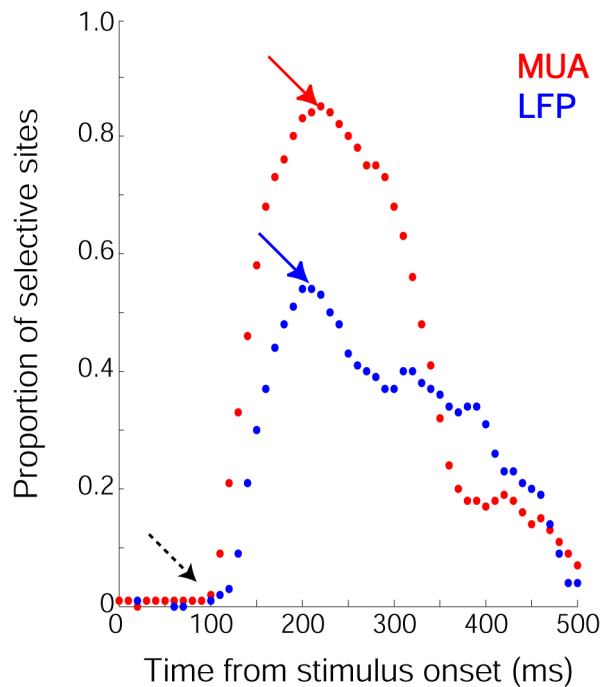
Example of the LFP responses at one IT recording site to the 77 different images. This is the same site shown in Figure 1 in the main text; here we show the responses to all 77 objects. The gray lines show the LFP response to each of the 10 repetitions of each stimulus aligned at the time of stimulus onset (the raw signal is low pass filtered at 300 Hz and the DC component is removed). The thick red line shows the average LFP waveform. The vertical dashed lines denote stimulus onset and offset. The ratio of the variance across images to the variance within images for the total power for this site was 4.4 (ANOVA $p < 10^{-8}$). A post-hoc t test to compare the responses during the 100 to 200 ms interval after stimulus onset to the baseline before stimulus presentation was applied to the LFP responses to the individual images (see Experimental Procedures, ‘**’ denotes $p < 0.001$ and ‘*’ denotes $p < 0.01$).



Supplementary Figure 2: Different frequency components of the LFP responses

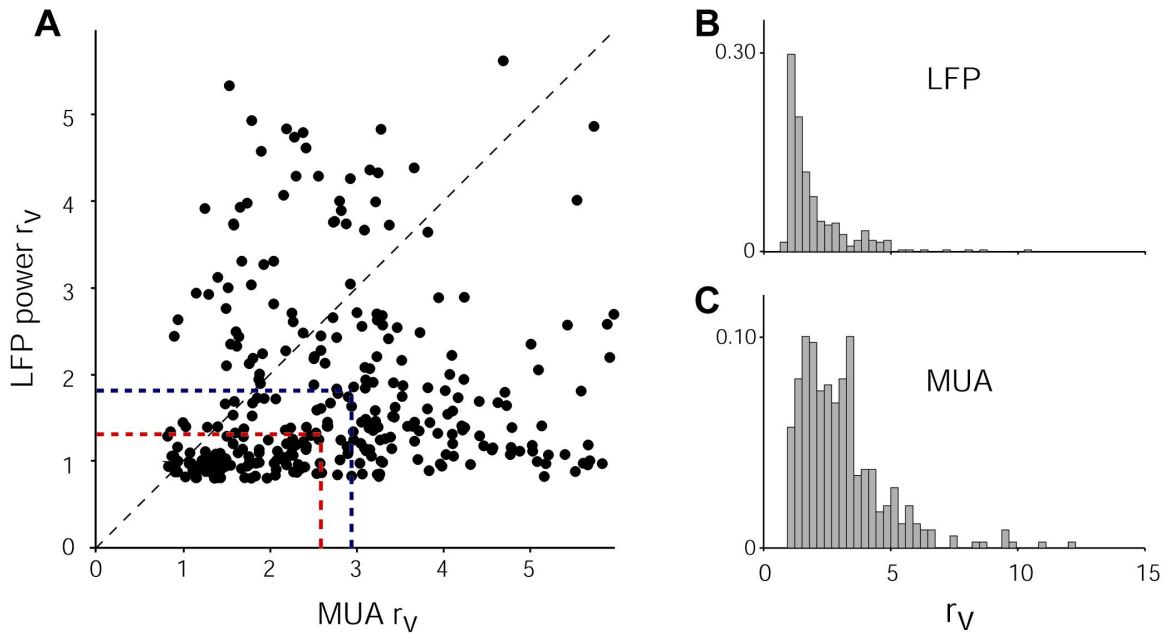
(A) Power spectral density of the LFP responses averaged across sites ($n=139$) and images. We computed the power spectral density using the Welch method with a 256-point Hanning window using a 10 point overlap (Press et al., 1996). For each site, the power was normalized by the maximum across images; the error bars show s.d. across sites. The small dip at 60 Hz is an artifact of the digital notch filter applied on the data.

(B) Proportion of LFP recording sites ($n=315$) that showed significant selectivity (1-way ANOVA, $p<0.001$) for the LFP power in different frequency bands of the LFP signal (see Experimental Procedures). We also show the corresponding proportion using the amplitude of the LFP signal as the definition of LFP response.



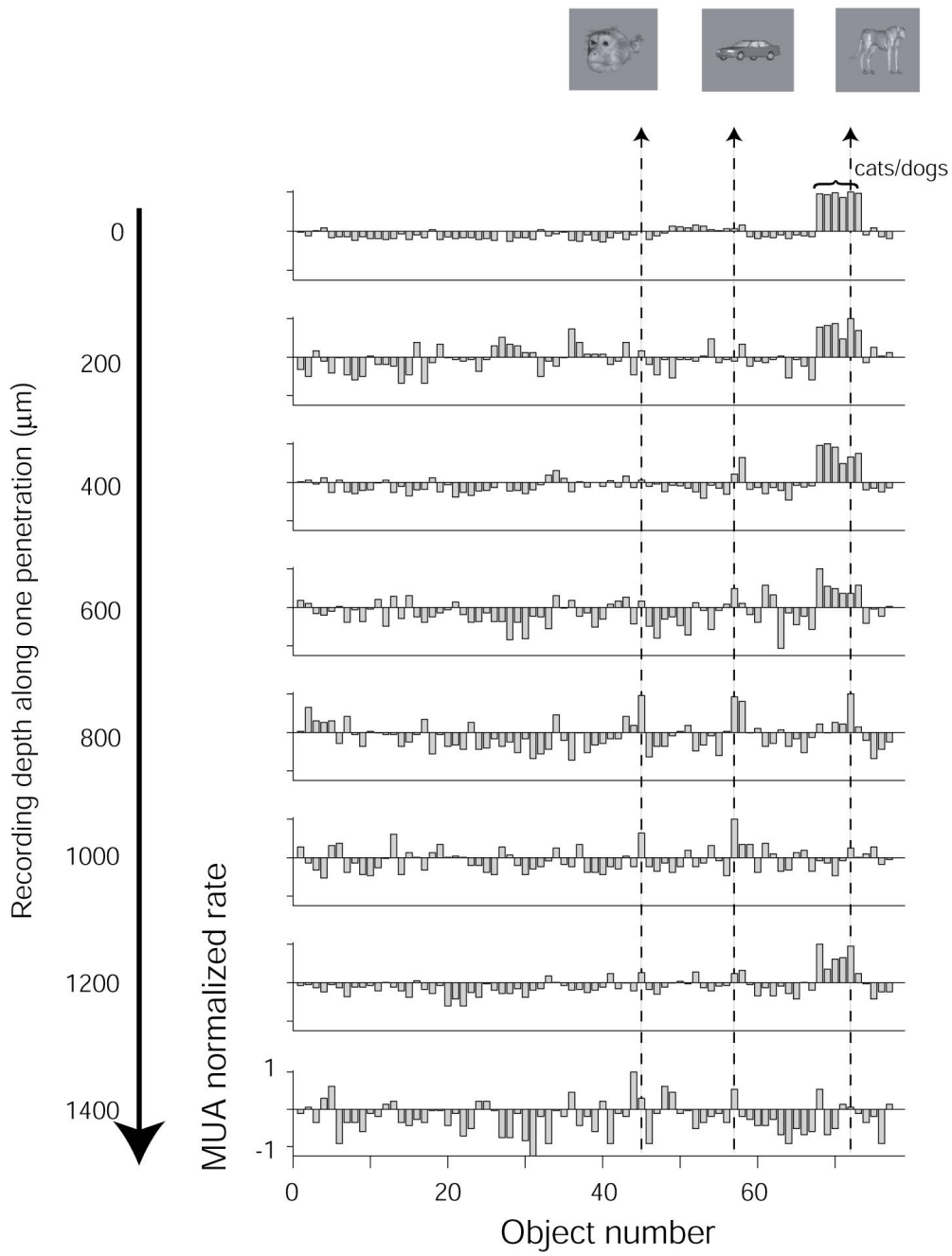
Supplementary Figure 3: Proportion of selective sites as a function of the response analysis window

Responses were defined in a sliding window (step = 10 ms) of 100 ms *ending* at the time indicated on the x-axis. For each window, we performed a one-way ANOVA ($p < 0.001$) to determine whether a site was selective or not. The y-axis indicates the proportion of sites that showed a selective response for MUA (red) and LFP (blue). The dotted arrow shows the proportion of selective sites for the [0;100) ms interval and the red and blue arrows indicate the maxima of the MUA and LFP curves respectively.



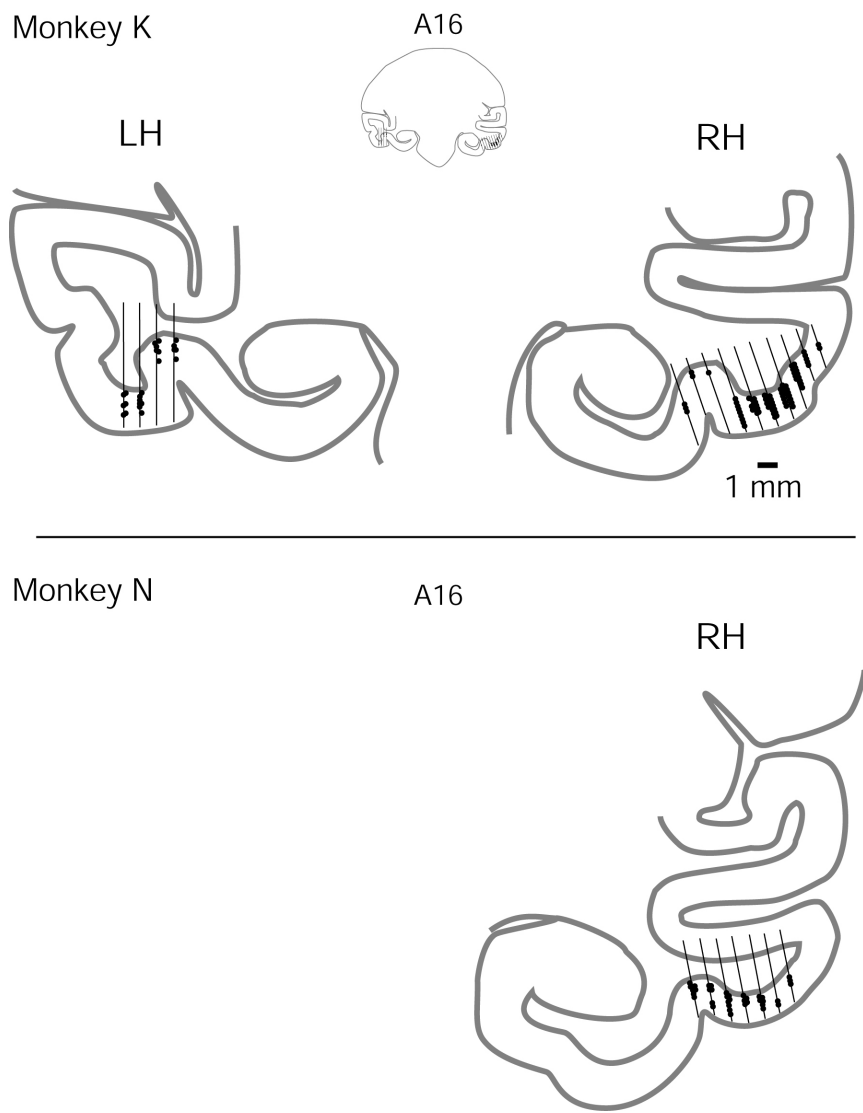
Supplementary Figure 4: Sharpness of MUA and LFP stimulus selectivity

A. Sharpness of the stimulus selectivity (ratio of the variance across pictures to the variance within pictures, r_v , see Experimental Procedures) for LFP power (ordinate) and the MUA spike counts (abscissa). The diagonal dashed line shows equivalent MUA and LFP selectivity. We show the median (red) and mean (blue) of the r_v distributions for the MUA and LFP ($n=249$ including selective and non-selective sites). The axis was cut at $r_v=6$ for clarity. The distributions of r_v values are shown in panel **B** (LFP) and panel **C** (MUA).



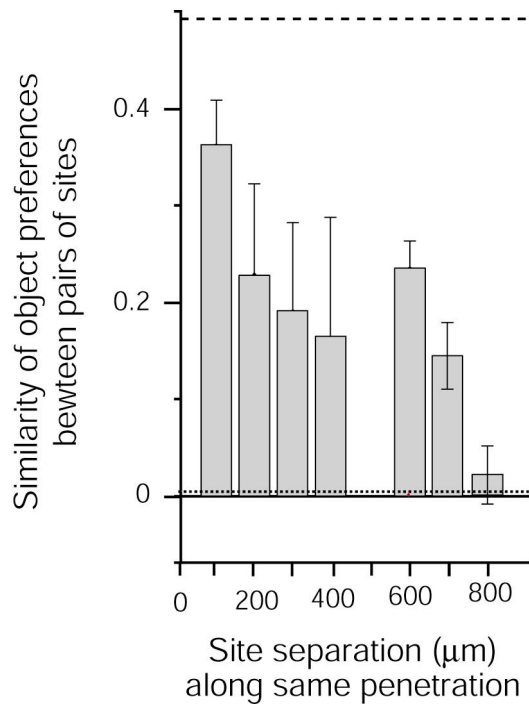
Supplementary Figure 5: Example of MUA responses in multiple sites during one penetration

Normalized spike response to each of the 77 images for 8 sites separated by 200 μm steps recorded along one penetration through ventral IT. For each site, the ordinate was computed by subtracting the average spike response to all images from the spike response to each image and then dividing by the maximum spike response (in the 100 to 300 ms interval following stimulus onset). The images are arranged along the abscissa in the same order as shown in Figure 1; the dashed lines highlight the responses to three example images shown at the top. The recording depth of each site is indicated to the right of the plot, and more superficial cortical layers are at the bottom of the plot.



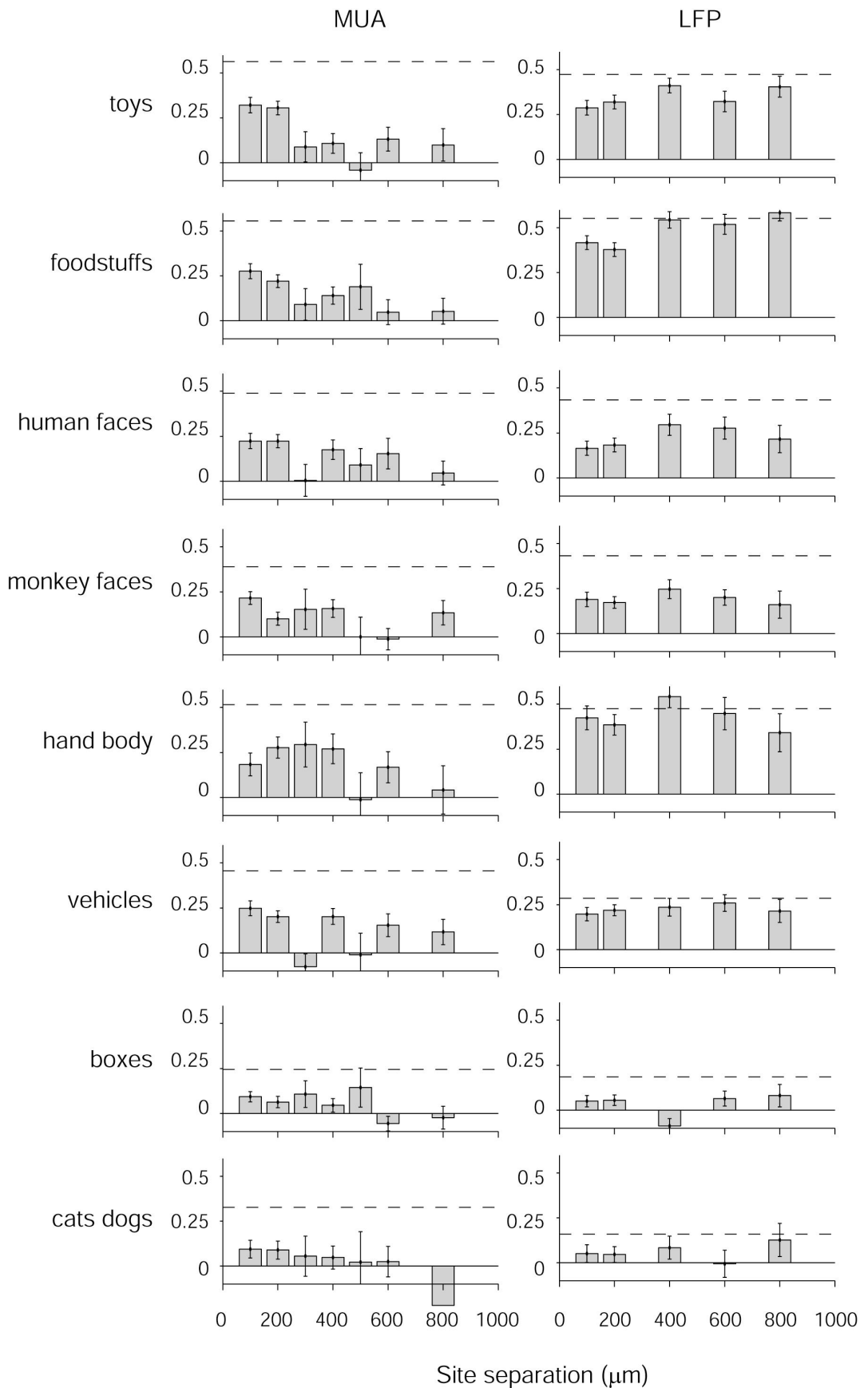
Supplementary Figure 6: Coronal MR site map

Estimates of electrode penetrations (lines) and recording site locations (dots) are drawn based on MR images from both monkeys taken after chamber implantation. Electrode penetrations were spaced 1 mm apart using a fixed grid at the surface of the skull and true tracking of each penetration was assisted by a guide tube that extended to within 20 mm of the ventral surface. The coronal sections at A16 are shown with recording sites for A15–A17. Only the right hemisphere was recorded in monkey N. Map topography was confirmed by the audible transitions between gray and white matter and by the depth of electrode travel before reaching the ventral surface and (in some cases) the dura beyond the ventral surface. Recording sites were estimated on this plot based on the point of physiologically assessed entry in the gray matter of the ventral surface. Note that electrode tracks were generally aligned along the columnar axis, and fewer recordings were made where alignment was poor.



Supplementary Figure 7: Similarity of SUA responses for nearby recording sites

The ordinate shows the mean Pearson correlation coefficients between responses to all 77 images at spatially separate sites as a function of the separation distance within the same penetration for single unit activity (the format is the same as in Figure 7). The distance between each pair of sites was determined by the microdrive readings along the penetration. As an estimate of the maximum correlation that could be expected given the variability in the data, the dashed horizontal line shows the mean correlation obtained from comparing the odd and even repetitions of the SUA vs. SUA at the same site (after correction for the number of repetitions). The dotted line shows the correlation coefficient between sites in different hemispheres.



Supplementary Figure 8: Similarity in responses *within* individual groups of pictures for nearby sites

This figure extends the observations in Figure 7 where correlations were computed between all 77 pictures. Here we compute the correlation coefficients for MUA (left) and LFPs (right) only *within* each of 8 specific groups of pictures: toys (9 images), foodstuffs (12 images), human faces (10 images), monkey faces (11 images), hand/body (4 images), vehicles (12 images), boxes (13 images) and cats/dogs (6 images). All the images are shown in Figure S1. The format is the same as in Figure 7.